# On Baseline Corrections and Uncertainty in Response Spectra for Baseline Variations Commonly Encountered in Digital Accelerograph Records

By Sinan Akkar and David M. Boore

## Abstract

Most digital accelerograph recordings are plagued by long-period drifts, best seen in the velocity and displacement time series obtained from integration of the acceleration time series. These drifts often result in velocity values that are nonzero near the end of the record. This is clearly unphysical and can lead to inaccurate estimates of peak ground displacement and long-period spectral response. The source of the long-period noise seems to be variations in the acceleration baseline in many cases. These variations could be due to true ground motion (tilting and rotation, as well as local permanent ground deformation), instrumental effects, or analog-to-digital conversion. Very often the trends in velocity are well approximated by a linear trend after the strong shaking subsides. The linearity of the trend in velocity implies that no variations in the baseline could have occurred after the onset of linearity in the velocity time series. This observation, combined with the lack of any trends in the pre-event motion, allows us to compute the time interval in which any baseline variations could occur. We then use several models of the variations in a Monte Carlo procedure to derive a suite of baseline-corrected accelerations for each noise model, using records from the 1999 Chi-Chi earthquake and several earthquakes in Turkey. Comparisons of the mean values of the peak ground displacements, spectral displacements, and residual displacements computed from these corrected accelerations for the different noise models can be used as a guide to the accuracy of the baseline corrections. For many of the records considered here the mean values are similar for each noise model, giving confidence in the estimation of the mean values. The dispersion of the ground-motion measures increases with period and is noise-model dependent. The dispersion of inelastic spectra is greater than the elastic spectra at short periods, but approaches that of the elastic spectra at longer periods. The elastic spectra from the most basic processing, in which only the pre-event mean is removed from the acceleration time series, do not diverge from the baseline-corrected spectra until periods of 10 to 20 s or more for the records studied here, implying that for many engineering purposes elastic spectra can be used from records with no baseline correction or

filtering.

## Introduction

Reliable long-period spectral information has become an important issue in earthquake engineering and engineering seismology. The information derived from long-period ground motion can be used in understanding the source- and path-related specific features of far- and near-fault ground motions (e.g. Jousset and Douglas, 2007; Somerville, 2003; Spudich and Chiou, 2008; Somerville et al., 1997); a detailed seismological overview of long-period ground motions is given in Koketsu and Miyake (2008). In structural engineering reliable long-period information is required for robust deformation-demand estimates of structural systems, particularly with the increased interest in displacement-based design and the emergence of nonlinear structural-response analyses (ATC, 2005). In recognition of the need for ground-motion estimations at longer periods, recent ground-motion prediction equations (GMPEs) have extended their spectral estimations to periods well above those in previous GMPEs (e.g. Boore and Atkinson, 2008; Campbell and Bozorgnia, 2008; Akkar and Bommer, 2007; Faccioli et al., 2004; Cauzzi and Faccioli, 2008). Furthermore, direct estimation of peak nonlinear oscillator displacements through GMPEs requires the specification of ground motion at long periods (e.g. Tothong and Cornell, 2006; 2008, Akkar and Küçükdoğan, 2008; Borzi et al., 2001).

The main obstacle to obtaining long-period ground motions is the noise in accelerometer records. By "noise" we mean any distortion to the signal that can lead to apparent errors in long-period motions when analyzed in the usual way. The source of the "noise" can be true ground motion due to dynamic rotation and tilting produced by wave propagation, inelastic motions due to local ground failure, amplitude-dependent transducer behavior, or even analog-to-digital conversion (e.g., Boore, 2003). It is not necessarily distributed in a stationary manner throughout the record, but can be confined to narrow-duration segments of the time series. This noise is embedded in records from both analog and digital accelerographs, although the character of the noise is usually different for the two types of records, as discussed by Boore and Bommer (2005) in detail (Figure 1). The noise is easiest

to see in displacement time series, where it most often takes the form of wavering, difficult-to-characterize motions in analog records. In digital records, however, the noise is generally much easier to describe: it appears as a drift in displacement, corresponding to one or several linear trends in velocity. The velocity does not approach zero at the end of the record, which is impossible on physical grounds. The form of the noise in digital records suggests that it is due small variations in the acceleration baseline, often occurring as near-instantaneous shifts in the baseline level.

The strategies for dealing with the long-period noise ranges from doing nothing to trying to correct for the baseline offsets. In the do-nothing case, measures of ground-motion intensity are computed from the zeroth-order-corrected (zoc) acceleration record (corresponding to a mean being removed from the record, the mean being from the pre-event portion of the record, usually available for digital recordings, or the whole record if not available), with the assumption that the noise only affects periods greater than a certain period ($T_{MAX}$). If a precise description of the noise exists, then it is possible, at least in theory, to correct for the noise and recover signal at long periods [e.g. Boroscheck and Legrand (2006) and Pillet and Vireux (2007) proposed methods to recover the true ground motion using models of tilt]. If such a description does not exist (as is usually the case for analog records), then low-cut filtering, with or without removal of low-order polynomials fit to the data, is the most commonly used adjustment method (Lee et al., 1982)[in such a case "correction" is too strong a term, for no correction is being made for the noise; both the signal and the noise are lost for periods greater than some fraction of the filter period and consequently true ground motion cannot be described (Trifunac and Todorovska, 2001)]. The polynomial fits are a form of baseline adjustments and as such amount to some type of low-cut filtering, although the equivalent filter is poorly defined in terms of the frequency response. For all cases of filtering with or without baseline adjustment, good practice involves the specification of a maximum period ($T_{MAX}$) above which the response spectra should not be used in engineering analyses or development of ground-motion prediction equations; $T_{MAX}$ is usually taken as a fraction of the filter period (e.g., Abrahamson and Silva, 1997; Akkar and Bommer, 2006)

The use of $T_{MAX}$ to decide whether or not response spectral ordinates are to be used in analyses is equivalent to assuming no error in the response spectra for periods less than $T_{MAX}$, and infinite error for periods greater than $T_{MAX}$. This assumption is one of the motivations for

this paper--we investigate a method for determining the error in the response spectra as a function of period, thinking that in future studies response spectra could be used without assuming a binary nature of the spectra--either usable or not usable. (A matter of terminology here: as we will be concerned only with long-period response spectra, we will be discussing and illustrating elastic, $SD_E$, and inelastic, $SD_{IE}$, displacement response spectra; $SD$ with no subscript is assumed to be elastic displacement response). In this paper we exploit what appears to be a common model of the noise: the velocity is often quite linear after the strong shaking subsides. A linear trend in velocity implies that any baseline variations must have occurred before the start of the linear trend. Our original goal was to define a period-dependent dispersion measure for records for which this noise model applies (and this means that from now on we will be concerned with the noise in digital records only). Our approach is to do Monte Carlo simulations for several models of the acceleration baseline variations, subject to two constraints: 1) these variations take place in a specified time interval and 2) the integrated effect of the offsets match the long-period trends after the specified time interval. We found that even though the simple noise model applies to many records, we were not successful in estimating a robust, noise-model-independent estimate of the dispersion in the long-period portion of the response spectra. On the other hand, for many records the mean residual displacement ($d_{RSDL}$) and the mean displacement response spectrum at long period is relatively stable and independent of the noise model. Thus our contribution in this paper is actually a Monte Carlo-based baseline-correction method that can be used to give some confidence in spectral displacements at periods longer than would normally be considered (and longer than for records for which only a zeroth-order-correction had been made). In addition, our results can be used to help define $T_{MAX}$, and we describe a robust way of determining some critical times in the modified Iwan baseline-correction (blc) method that is useful even if our Monte Carlo correction method is not used.

## Determination of Times for Modified Iwan BLC

Our investigation is founded in the Iwan et al. (1985) baseline adjustment procedure for removing long-period noise from accelerograms. Even though we do not apply their method directly in this paper, we find it useful to discuss their method, as many of its features are used in our analysis. In addition, we propose a way of choosing constraints on some times

that are essential components of the Iwan et al. (1985) method as generalized by Boore (2001). The method assumes that variations in the acceleration baseline are confined to times between $t_1$ and $t_2$, where $t_2 > t_1$. This differs from previous baseline correction procedures that assumed the noise to be distributed throughout the acceleration time series. Although complex baseline variations can occur between these two times during the interval of strong ground shaking, the accumulated effect of these variations is represented by a single average offset in the baseline, $a_m$ (Figure 2). This offset is then followed by another constant offset $a_f$ extending from $t_2$ to the end of the record. This second offset can be determined either by fitting a line to the velocity obtained from a single integration of the zeroth-order-corrected (zoc) acceleration (hereinafter called the "zoc velocity") or by fitting a quadratic to the zoc displacement (computed by double integration of the zoc acceleration). In either case, the fit is done using a least-squares fit to the appropriate time series between beginning and ending times $t_{FITb}$ and $t_{FITe}$ (determining a baseline correction by fitting a portion of the record was first advocated by Graizer, 1979). Thus there are four times to be specified in the Iwan et al. (1985) correction procedure: $t_1$, $t_2$, $t_{FITb}$, and $t_{FITe}$. The time $t_{FITe}$ is usually chosen to be the end of the record ($t_{FITe} = t_{END}$) whereas $t_{FITb}$ is set subjectively to a time well after the strong shaking has subsided (we will discuss shortly a less subjective procedure for choosing $t_{FITb}$). Iwan et al. (1985) chose $t_1$ and $t_2$ based on laboratory testing of the specific instrument with which they were concerned; Boore (2001) generalized their method by allowing $t_1$ and $t_2$ to be free parameters, subject to the constraints that $t_1 > 0$, $t_2 > t_1$ and $t_2 < t_{END}$. A particularly simple end-member of this generalization assumes a single offset at a time ($t_{V0}$) given by the intersection of the line fit to the final portion of the zoc velocity with the zero axis, in which case $t_1 = t_2 = t_{V0}$. This further modification to Iwan et al.'s original method is termed by Boore (2001) the "v0 correction." Boore (2001) showed that the residual displacements (the essentially flat level of the displacement time series near the end of the record, which might be interpreted as the co-seismic displacement of the ground due to slip on the fault) can be sensitive to $t_2$, leading him to be pessimistic about the general ability of the modified Iwan method to remove long-period noise (Figure 3). This was contrary to the finding for the Chi-Chi earthquake that the residual displacements derived using the modified Iwan procedure, usually the v0 correction, were in good overall agreement with the coseismic displacements from GPS (e.g. Oglesby and Day, 2001; Wu and Wu, 2007; see also Figure C.4 in Boore and Atkinson, 2007, which shows that double integration of the TCU074

record without any baseline correction yields residual displacements close to those from the GPS measurements). What Boore (2001) did not consider is that there is a constraint on $t_2$: it cannot be greater than the time beyond which the zoc velocity is essentially linear. In this paper we take advantage of this constraint to determine the maximum time, $t_{BLe}$, for $t_2$; values of $t_2$ beyond $t_{BLe}$ would imply a nonlinear zoc velocity, contrary to the way that $t_{BLe}$ is determined ("*BLe*" stands for "*B*ase*L*ine *e*nd": the end of the time interval in which baseline variations can take place). In a similar way, we define $t_{BLb}$ as the time before which there are no obvious baseline variations; this sets the minimum time for $t_1$ ("*BLb*" stands for "*B*ase*L*ine *b*eginning"). With $t_{FITe} = t_{END}$, we now have two times to determine: $t_{BLe}$ and $t_{FITb}$. We discuss the determination of these times in the rest of this section, starting with $t_{FITb}$.

$t_{FITb}$ should be chosen well after the strong shaking has ceased, but if chosen too close to the end of the record the fitted function will be sensitive to the value of $t_{FITb}$ and thus will not provide a robust and stable estimation of the noise trend (but if little post-event record is available, the whole procedure we discuss here is compromised, as then it will not be possible to find a reliable trend due to noise). We use an iterative procedure to determine $t_{FITb}$. We start by choosing $t_{FITb}$ to be an increment $\Delta$ less than $t_{FITe}$, and then we find $a_f$ by fitting either a first-order polynomial to zoc velocity or a second-order polynomial to zoc displacement (we illustrate the procedure here with fits to zoc velocity because it is easier to visualize, but we found that the residual displacements are flatter when determined from zoc displacement, and thus we used fits to zoc displacement in the next section). We then reduce $t_{FITb}$ by $\Delta$ and determine a new $a_f$. Thus, for example, for iteration $i$ we fit $v_i = v_{0,i} + a_{f,i}t$ to zoc velocity from $t_{FITb} = t_{FITe} - i\Delta$ to $t_{FITe}$. We plot the ratios of consecutive slopes ($a_{f,i+1}/a_{f,i}$) against $t_{FITb}$. The time at which these ratios attain a relatively constant level of unity is taken as the value of $t_{FITb}$ for subsequent analysis. Note that we are not trying to determine if a linear trend is the best model for the later part of the zoc velocity; we assume that it is. This is probably a poor assumption for very long records, because other noise sources not related to the earthquake of interest can introduce variations in the acceleration baseline. In such cases $t_{FITe}$ should be chosen at a time less than $t_{END}$. We realize that there may be more sophisticated statistical procedures to accomplish our goal of finding a robust fit to the noise trend, but what we have described is simple, intuitive, and seems to work.

We determine $t_{BLe}$ on the basis of increasing variations of the zoc velocity from the line corresponding to $t_{FITb}$, working toward decreasing time from $t_{FITb}$. The idea here is to find the time beyond which the zoc velocity has little variation about a linear trend, implying that there is little change in the ground shaking. We again use an iterative procedure, extending the line fitted to zoc velocity from $t_{FITb}$ (determined in the previous paragraph) towards decreasing time in increments of $\Delta$. We plot the standard deviations between the fitted line and the zoc velocity for the time interval $[t_{FITb} - i\Delta, t_{FITb}]$ as a function of $t_{FITb} - i\Delta$. We set $t_{BLe}$ as the value of $t_{FITb} - i\Delta$ for the iteration where there is an abrupt increase in the standard deviation (baseline variations could occur for earlier times than $t_{BLe}$). It is important to emphasize that the time $t_2$ in the modified Iwan et al. baseline correction procedure is not necessarily equal to $t_{BLe}$; all we can say is that $t_2 \leq t_{BLe}$. The determination of $t_{BLb}$ is similar to that for $t_{BLe}$. In this case the trend of the zoc velocity with respect to which the standard deviation is computed is simply the zero line, as visual inspection of the zoc velocity usually shows little or no divergence from a value of 0.0 for times less than the *P*-wave arrival. The iterations proceed in a forward fashion, so that the time interval used for the standard deviation computation is $[0, i\Delta]$.

An illustration will help clarify our procedure. Figure 4 shows these iterative steps by using the EW component of the TCU068 station from the 1999 Chi-Chi, Taiwan earthquake. The zoc velocity (top graph) shows a physically unrealistic, monotonically increasing linear trend after the strong pulse that dominants the waveform. The second graph shows the slope ratios of the iterative straight line fits (i.e., $a_{f,i+1}/a_{f,i}$) for various choices of $t_{FITb}$, in increments of 1 s ($\Delta$ = 1 s). The ratios diverge from unity for times greater than 63 s, and thus $t_{FITb}$ is taken as 63 s for this record. The third graph shows the standard deviation computations as a function of $t_{BLe}$. There is an abrupt change in the standard deviation for times less than about 43.0 s (note that this time also corresponds to the divergence of $a_{f,i+1}/a_{f,i}$ from unity for decreasing times, which may be an alternative way of determining $t_{BLe}$). A change of slope in zoc velocity, corresponding to a baseline offset, does not necessarily occur at this time, but natural swings in the velocity due to true ground motion obscure any slope changes for times less than $t_{BLe}$; what we can say is that any changes in slope after $t_{BLe}$ are small, and thus $t_{BLe}$ is an upper bound for the time interval in which baseline variations can occur. The bottom graph shows the basis for determining $t_{BLb}$. The standard deviation has an abrupt increase starting at about 31.0 s, and thus we chose $t_{BLb}$ as

this time. Based on this analysis, for this record the maximum time interval in which baseline variations in acceleration might occur is 31.0 s to 43.0 s. In the next section we discuss a baseline correction scheme that makes use of this interval as a constraint on the corrections.

Clearly choosing $t_{BLb}$ and $t_{BLe}$ does involve subjective judgment as to when the standard deviations increase rapidly. We note that there are small increases in the standard deviations before and after the times we chose for $t_{BLb}$ and $t_{BLe}$. These increases are associated with the P-wave arrival and the decreasing coda for $t_{BLb}$ and $t_{BLe}$, respectively. We ignore these, looking for more rapid increases in the standard deviations.

## Baseline Corrections and Estimation of Elastic Spectra and Dispersion for Four Noise Models

Using the results from the previous section, we have constraints on the time interval in which baseline variations could have taken place, as well as the important constraints of the final offset, $a_f$, and the integrated value of all baseline variations at time $t_{BLe}$ ($v(t_{BLe})$: the equation of the line fit to the zoc velocity evaluated at $t = t_{BLe}$). To proceed farther, however, requires specific models for the baseline variations that could have occurred within the [$t_{BLb}$, $t_{BLe}$] time interval. Our procedure is to consider four increasingly complex models of the variations. For each model we generate random variations consistent with the constraints, and for each simulation we correct the zoc acceleration by subtracting the negative of the acceleration baseline offsets, after which we compute baseline-corrected velocities, displacements, and response spectra. We then compute the arithmetic mean of the displacements to estimate peak displacements ($PGD$) and residual displacements and the geometric mean of the displacement response spectra to obtain a robust estimate of $SD$ at long periods. Our initial goal was to derive a good estimate of the uncertainty in $PGD$ and $SD$, but we found those quantities to be dependent on the noise model. We did find, however, that often the mean $PGD$ and $SD$ are relatively insensitive to the noise model, in which case we have confidence in the baseline-corrected mean values from our procedure. This was an unintended success that was not the prime motivation for doing this study.

The four noise models used in our study are shown in Figure 5. The first model (M1)

assumes a single constant offset in the acceleration baseline between $t_{BLb}$ and $t_{BLe}$ whose location and amplitude is determined by implementing the v0 correction. The second model (M2) is the baseline variation model of Paolucci et al. (2008), with a ramp baseline offset over the time interval $[t_{r1}, t_{r2}]$. The third model (M3) assumes an constant average drift ($a_{m1}$) over a time interval $[t_{r1}, t_{r2}]$. The last model (M4) is a more complex version of M3 having two consecutive constant offsets ($a_{m1}$ and $a_{m2}$) between the intervals $[t_{r1}, t_{r2}]$ and $[t_{r2}, t_{r3}]$. Some of the key parameters necessary for each baseline-variation model are determined in a random manner through Monte Carlo simulations, assuming a normal distribution of the random variables, with the other parameters determined by the constraints mentioned above (the rules implemented for determining these parameters are presented in Figure 5 next to each model plot).

To implement the procedure, we used the ground motions presented in Table 1. We chose these records for several reasons: the 1999 Chi-Chi records are large amplitude and are known to have linear trends in the zoc velocity; the other records, from earthquakes in Turkey, are smaller in amplitude but also have linear trends in velocity (see Akkar et al., 2005, for an in-depth analysis of the Bingöl record). For each record we determined $t_{BLb}$, $t_{BLe}$, $a_f$, and $v(t_{BLe})$. These were held fixed (the times are listed in Table 1). The M1 model was entirely determined from these values. For the other models we performed Monte Carlo simulations to determine baseline offsets for a suite of 100 realizations; Figure 6 shows a set of these realizations for the TCU076-EW record. We then corrected the zoc acceleration by subtracting the negative value of each baseline offset, and then computed the velocity and displacement time series and the response spectrum, as well as the means as described above. We note that each simulation satisfies the physical condition that the final baseline-corrected velocity averages to zero. Figures 7, 8, and 9 show some examples of the estimated ground displacements, 5%-damped response spectra ($SD_E$) and corresponding dispersion from the Monte Carlo simulations. Spectral displacements are computed up to a period of 500 seconds to cover, in a practical sense, the full effect of long-period noise and to capture the peak ground displacement (see also the Appendix). The dispersion of the spectra is described by the standard deviation of natural logarithm of $SD_E$. The figures illustrate increasing sensitivity to the noise models, with the records least and most sensitive to the noise models shown in Figures 7 and 9, respectively. For comparison, the figures include the zoc

displacements and $SD_E$, as well as the mean displacements and $SD_E$. In looking at the figures it is useful to keep in mind that the long-period $SD_E$ is controlled by $PGD$, as discussed in the Appendix. This means that the variability in the long-period $SD_E$ is directly related to the variability of $PGD$, as can be seen by comparing the bottom graphs in each figure with the $PGD$ variability shown by the short horizontal gray line. We see that the variability of $SD_E$ increases rapidly with period, usually attaining a plateau for periods beyond about 100 s. The variability of $SD_E$ also increases with the complexity of the source model, which means that we cannot attain our initial goal of characterizing the period-dependent uncertainty of $SD_E$. We hoped that such a characterization could be used by analysis methods (such as those for obtaining ground-motion prediction equations or analyzing the statistics of displacement-based structural response) that could take advantage of such period-dependent information, rather than the usual "use/don't use" methods, for which $SD_E$ is assumed to be error free below a certain period and so uncertain above that same period as not to be useful. On the other hand, the mean of both the residuals displacements and the long-period $SD_E$ are often quite similar for the various noise models, which we find encouraging. This model-independence implies that the Monte Carlo-based baseline-correction procedures are giving reliable estimates of the response spectra at periods much longer than would be inferred from the period at which the $SD_E$ from the zoc acceleration diverges from the $SD_E$ from the baseline-corrected accelerations. Often the simplest correction based on the M1 noise model provides results comparable to the more complex models.

We present the displacements and $SD_E$ for all records in Figures 10 and 11. The average $PGD$, and their uncertainties, are given in Table 1. Note that for some cases there are no entries for the M1 and M2 noise models because the constraints for these models could not be met. For the Bolu (NS) record the intersection of the velocity line with the zero axis (used in the M1 noise model) occurred at negative times. The blank entries for the M2 model are because the signs of the final offset, $a_f$, and the velocity line at $t_{BLe}$, $v(t_{BLe})$, were not the same, which is a logical impossibility for the model given the constraints on $t_{r1}$ and $t_{r2}$ (see Figure 5). The results in Figures 10 and 11 and Table 1 are consistent with the conclusions that we drew from the three records analyzed in Figures 7, 8, and 9. The $PGD$ (and

therefore the long-period $SD_E$) are very similar from noise model to noise model for a number of records, and the standard deviation of $PGD$ (and therefore the long-period $SD_E$) increases with the complexity of the noise model.

The residual displacements (the essentially flat portions of the baseline-corrected displacements at late times) usually do not affect the $SD_E$ (see the Appendix), but they can be important for studies of the slip on faults and can be of engineering interest while evaluating the structures near active faults that crop out or come close to the surface, for which significant spatial variations in residual displacement can be expected. The displacements can be seen in Figure 10, with the mean values and the variation given in Table 2. As with $PGD$ and long-period $SD_E$, the mean values are often relatively insensitive to the noise model. Table 2 also contains residual displacements from the baseline correction method developed for the estimation of permanent ground displacements by Wu and Wu (2007). They used a modification of the Iwan et al. (1985) method that chose some of the times using subjective judgment in combination with a flatness criterion. Estimates of coseismic displacement from nearby GPS stations are also given in Table 2, along with the distance from the GPS station to the accelerograph station. The Wu and Wu residual displacements are often in better agreement with the GPS values than ours. We assume that their baseline corrections were done with no knowledge of the GPS displacements. But we also point out that there can be considerable spatial variation in the GPS values. This is best seen in Table 3, which lists the GPS coseismic displacements from four GPS stations located on the hanging wall of the 1999 Chi-Chi mainshock rupture surface, at approximately the same distance from the fault. As can be seen in the table, the variation is significant between GPS stations separated about the same distance as the GPS station and accelerographs. Given the spatial variability and the fact that residual displacements have little effect on long-period $SD_E$, we think that the residual displacement comparisons are of less interest than the peak displacement and $SD_E$ comparisons for most engineering purposes.

## Long-Period Noise Influence on Nonlinear Spectra

We used the suite of baseline-corrected accelerations to study the variability of inelastic response as a function of period, using the M4 noise model. There are indications from

previous studies that inelastic spectra can be sensitive to long-period processing details at shorter periods than elastic spectra (e.g., Boore and Akkar, 2003). We used a nonlinear oscillator with 5%-damped elastoplastic hysteretic behavior (i.e. no post-elastic stiffness). This hysteretic behavior is widely used for modeling the steel structural systems. We chose an elastic strength to yield strength ratio (i.e. $F_E/F_Y$) of 4 for the oscillator, which corresponds to a moderate-strength structural system. This type of spectrum is known as constant strength spectrum and it is widely used in the seismic performance assessment of structural systems. [The reader is referred to ATC (2005) for detailed information about the nonlinear oscillator response and types of nonlinear spectrum]. The spectra were computed up to 500 seconds for comparison with their elastic counterparts. The nonlinear oscillator response at each vibration period was solved numerically using the Newmark beta method, using $\beta = 1/6$ (USDP, 2008). Figure 12 compares the elastic (left panel) and inelastic (middle panel) spectral displacements together with the corresponding dispersions (right panel) represented as period-dependent logarithmic standard deviations. The comparisons are presented for the M4 noise model baseline corrections of 3 particular records (TCU052-NS, TCU076-EW and LDEO375-NS). The M4 noise model was chosen because it led to more variability in the response spectra at long periods. As in Figures 7, 8, and 9, we chose the records based on the variability of the long-period elastic spectra, with TCU052-NS having the least sensitivity and LDEO375-NS having the most sensitivity. The most important observation from these comparative plots (particularly the variability plots in the last column of graphs in Figure 12) is that the influence of long-period noise on inelastic response spectrum commences at periods significantly shorter than the corresponding elastic system, with several times more uncertainty in the inelastic spectra at periods less than 10 s than in the elastic spectra. The standard deviations of both the elastic and the inelastic spectra follow each other very closely for periods greater than 10 or 20 s, suggesting that the long-period noise influence is approximately the same for very flexible elastic and inelastic systems. This discussion clearly indicates that the response to long-period noise is different in elastic and inelastic systems and the differences are prominent at the periods of engineering interest. Therefore, different empirical and/or theoretical rules should be used for elastic and inelastic spectra in determining the period ranges where the long-period noise influence becomes important. To the best of our knowledge, rules proposed for determining the periods at which long-period noise influences the computed peak nonlinear oscillator response do not exist. (There are rules for reducing the filter cut-off influence on the computed elastic spectral quantities, such as Akkar and Bommer, 2006). In the absence of such rules, researchers investigating predictive

models for nonlinear response either reduce the spectral period ranges intuitively to decrease the likely long-period noise influence from the spectral calculations (e.g. Akkar and Küçükdoğan, 2008) or totally ignore this effect in their predictive models (e.g., Tothong and Cornell, 2006).

## Conclusions

Our main contribution in this paper is a Monte Carlo-based baseline correction procedure that can be used to give some confidence in spectral displacements at periods longer than normally considered in routine processing. Our procedure can be used to help define the period range of usable spectral displacements and might be used to avoid "use/don't use" decisions in which the spectral displacements are assumed to be error free for periods less than some $T_{MAX}$, yet have infinite error above that period. In addition, we describe a robust way of determining some critical times in the modified Iwan baseline-correction method. Our method can be used to assess the relative reliability of different recordings.

Our study is based on the observation that the long-period noise in digital accelerograph recordings is often in the form of a linear trend in the velocity time series after the strong shaking has ceased. If the long-period noise is due to variations in the acceleration baseline, then the linearity of this trend in velocity implies that no baseline variations could have occurred after the beginning of the linear trend. We use this observation to put constraints on the time interval in which baseline variations could have occurred, and we use Monte Carlo simulations subject to these constraints, for four models of the baseline variations, to find a suite of baseline-corrected acceleration time series. From these we computed velocity and displacement time series and elastic and inelastic response spectra. We find that the means of the peak ground displacements, the long-period spectral response, and the residual displacements are often relatively insensitive to the noise models used in the simulations, giving confidence in the determination of these measures of seismic intensity. Looked at the other way, differences of the mean values from the various noise models would imply that the values are not accurate, thus providing a way of judging the accuracy of the baseline corrections, at least in a qualitative way. The simplest baseline-correction procedure, which requires no simulations, often gives $PGD$ and $SD$ that compare well with those values from

the simulation-based correction procedures. $SD$ computed with the even the most basic zeroth-order-correction yields $SD$ that only diverge from the baseline-corrected $SD$ at periods greater than 10 or 20 s for the records studied here, consistent with the findings of Paolucci et al. (2008) and Cauzzi and Faccioli (2008).

The variability of the spectral displacements increases with period, but they are model dependent. The inelastic spectra show more variability than the elastic spectra at short periods, indicating that inelastic response spectra may be more sensitive to record processing procedures than elastic response spectra. The level of dispersion of the inelastic spectra becomes equal to that of elastic spectra at longer periods, as might be explained by the equal displacement rule. We note that nonlinear oscillator behavior is complex and a detailed investigation of the influence of long-period noise on the nonlinear oscillator response is not the major objective of our study. For the particular spectrum type (constant strength) and the records analyzed, we showed that the nonlinear spectrum can be more vulnerable to long-period noise for the periods of engineering interest. Therefore, the reliability of peak nonlinear deformation demands due to long-period noise should be treated cautiously. The rules implemented to describe the spectral bands for trustworthy peak elastic response may not be appropriate when the oscillator responds beyond the elastic range.

## Data and Resources Section

The Chi-Chi records used in this study are provided by the Central Bureau of Taiwan. The Turkish records are obtained from the 105G016 project funded by the Turkey Scientific and Technical Research Council.

## Acknowledgments

This study is financially granted by TUBITAK (Turkey Scientific and Technical Research Council) with the award no. 105G016. Mr. Abdullah Sandikkaya helped us for computing the $t_{BLe}$ and $t_{FITb}$ values from the iterative procedure described in the paper. We thank Chris Stephens for many discussions of record processing and Kent Fogleman, Basil Margaris, and Chris Stephens for useful reviews. We thank two anonymous reviews for constructive comments that resulted in improvements to the paper.

# References


Abrahamson, N. A. and W.J. Silva (1997). Empirical response spectral attenuation relations for shallow crustal earthquakes, *Seismol.Res. Lett.* **68**, 94-127.

Akkar, S. and B. Küçükdoğan (2008). Direct use of PGV for estimating peak nonlinear oscillator displacements**,** *Earthquake Engineering and Structural Dynamics* **37**, (in press).

Akkar, S. and J. J. Bommer (2006). Influence of long-period filter cut-off on elastic spectral displacements, *Earthquake Engineering and Structural Dynamics* **35**, 1145-1165.

Akkar, S. and J. J. Bommer (2007). Prediction of elastic displacement response spectra in Europe and the Middle East, *Earthquake Engineering and Structural Dynamics* **36**, 1275-1301.

Akkar, S., D. M. Boore, and P. Gülkan (2005). An evaluation of the strong ground motion recorded during the May 1, 2003, Bingöl, Turkey, earthquake, *J. Earthquake Engineering* **9**, 173—197.

Applied Technology Council (ATC) (2005). Improvement of nonlinear static seismic analysis procedures, Report FEMA-440.

Boore D. M. (2001). Effect of baseline corrections on displacement and response spectra for several recordings of the 1999 Chi-Chi, Taiwan, earthquake, *Bull. Seismol. Soc. Am.* **91**, 1199-1211.

Boore, D. M. (2003). Analog-to-digital conversion as a source of drifts in displacements derived from digital recordings of ground acceleration, *Bull. Seism. Soc. Am.* **93**, 2017—2024.

Boore, D. M. and S. Akkar (2003). Effect of causal and acausal filters on elastic and inelastic response spectra, *Earthq. Eng. and Struct. Dynamics* **32**, 1729—1748.

Boore, D. M. and G. M. Atkinson (2007). Boore-Atkinson NGA Ground Motion Relations for the Geometric Mean Horizontal Component of Peak and Spectral Ground Motion Parameters, *PEER 2007/01*, Pacific Earthquake Engineering Research Center, Berkeley, California. (available from http://peer.berkeley.edu/products/Boore-Atkinson-NGA.html).

Boore, D. M. and G. M. Atkinson (2008). Ground-motion prediction equations for the average horizontal component of PGA, PGV, and 5%-damped PSA at spectral periods between 0.01s and 10.0s, *Earthquake Spectra* **24**, 99-138.

Boore, D.M. and J.J. Bommer (2005). Processing of strong-motion accelerograms: Needs, options and consequences, *Soil Dyn. and Earthquake Eng.* **25**, 93-115.

Boroscheck, R.L. and D. Legrand (2006). Tilt motion effects on the double-time integration of linear accelerometers: an experimental approach, *Bull. Seism. Soc. Am.* 96, 2072–2089.

Borzi, B., G. M. Calvi, A. S. Elnashai, E. Faccioli, and J. J. Bommer (2001). Inelastic spectra for displacement-based seismic design, *Soil Dynamics and Earthquake Engineering* **21**, 47-61.

Campbell, K. W. and Y. Bozorgnia (2008). NGA ground motion model for the geometric mean horizontal component of PGA, PGV, PGD and 5% damped linear elastic response spectra for periods ranging from 0.01 to 10s, *Earthquake Spectra* **24**, 139-171.

Cauzzi, C. and E. Faccioli (2008). Broadband (0.05 to 20 s) prediction of displacement response spectra based on worldwide digital records, *J. Seismology* **12**, 453-475.

Faccioli, E., R. Paolucci and J. Rey (2004). Displacement spectra for long periods, *Earthquake Spectra* **20**, 347-376.

Graizer, V. M. (1979). Determination of the true ground displacement by using strong motion records, *Izvestiya Phys. Solid Earth* **15**, 875–885.

Iwan, W. D., M. A. Moser, and C.-Y. Peng (1985). Some observations on strong-motion earthquake measurement using a digital accelerograph, *Bull. Seism. Soc. Am.* **75**, 1225–1246.

Jousset, J. and J. Douglas (2007). Long-period earthquake ground displacements recorded on Guadeloupe (French Antilles), *Earthquake Engineering and Structural Dynamics* **36**, 949-963.

Koketsu, K and H. Miyake (2008). A seismological overview of long-period ground motion, *J. Seismology* **12**, 133-143.

Oglesby, D. D. and S. M. Day (2001). Fault Geometry and the Dynamics of the 1999 Chi-Chi (Taiwan) Earthquake, *Bull. Seism. Soc. Am* **91**, 1099-1111.

Paolucci, R., A. Rovelli, E. Faccioli, C. Cauzzi, D. Finazzi, M. Vanini, C. Di Alessandro and G. Calderoni (2008). On the reliability of long-period response spectral ordinates from digital accelerograms, *Earthquake Engineering and Structural Dynamics* **37**, 697-710.

Pillet, R. and J. Virieux (2007). The effects of seismic rotations on inertial sensors. *Geophys. J. Int.* 171, 1314 – 1323.

Somerville, P. G. (2003). Magnitude scaling of the near fault rupture directivity pulse, *Phys Earth Planet. Inter*. **137**, 201-212.

Somerville, P. G., N. F. Smith, R. V. Graves, and N. A. Abrahamson (1997). A modification of empirical strong ground motion attenuation relations to include the amplitude and duration effects of rupture directivity, *Seismol. Res. Lett.* **68**, 199-222.

Spudich, P. and B. S.-J. Chiou (2008). Directivity in NGA earthquake ground motions: Analysis using isochrone theory, *Earthquake Spectra* **24**, 279-298.

Tothong, P. and C. A. Cornell (2006). An Empirical Ground-Motion Attenuation Relation for Inelastic Spectral Displacement, *Bull. Seism. Soc. Am.* **96**, 2146-2164.

Tothong, P. and C. A. Cornell (2008). Structural performance assessment under near-source pulse-like ground motions using advanced ground motion intensity measures, *Earthquake Engineering and Structural Dynamics* **37**, 1013-1037.

Trifunac, T. and M. Todorovska (2001). A note on the usable dynamic range of accelerographs recording translation, *Soil Dyn. Earthquake Eng.* 21, 275-286.

Utility Software for Data Processing, USDP (2008). www.usdp.org

Wu, Y.-M. and C.-F. Wu (2007). Approximate recovery of coseismic deformation from Taiwan strong-motion records, *J. Seismology* **11**, 159–170.

Yu, S. B., L. C. Kuo, Y. R. Hsu , H. H. Su, C. C. Liu, C. S. Hou, J. F. Lee, T. C. Lai, C. C. Liu, and C. L. Liu (2001). Preseismic deformation and coseismic displacements associated with the 1999 Chi-Chi, Taiwan , earthquake, *Bull. Seism. Soc. Am.* **91**, 995 – 1012

# Contact Information

Sinan Akkar (SA)
Earthquake Engineering Research Center
Department of Civil Engineering
Middle East Technical University 06531
Ankara, Turkey
sakkar@metu.edu.tr

David M. Boore (DMB)
US Geological Survey MS 977
345 Middlefield Road
Menlo Park, California 94025
boore@usgs.gov

# List Of Tables

## Table 1.

Information about the digital accelerograms used in this study (see Data and Resources Section). The listed time values ($t_{BLb}$, $t_{BLe}$, and $t_{FITb}$) are from the method discussed and the mean peak ground displacements ($PGD$) are computed from the suite of 100 baseline-corrected accelerograms, for the three baseline-offset noise models M2 through M4. Only one displacement time series is associated with the deterministic noise model M1.

| Record | $M_w$, $R_{jb}$ (km), NEHRP site class | Record Length ($t_{FITe}$) (s) | $T_{BLb}$ (s) | $T_{BLe}$ (s) | $T_{FITb}$ (s) | Geometric Mean of PGD (cm) | | | | $\sigma_{ln(PGD)}$ | | | |
|---|---|---|---|---|---|---|---|---|---|---|---|---|---|
| | | | | | | M1 | M2 | M3 | M4 | M1 | M2 | M3 | M4 |
| LDEO0375 (NS)-12/11/99 | 7.2, 2.6, C | 42 | 11 | 28 | 29 | 32 | 23 | 55 | 64 | - | 0.249 | 0.523 | 0.823 |
| LDEO0375 (EW)-12/11/99 | 7.2, 2.6, C | 42 | 11 | 27 | 29 | 32 | 26 | 16 | 35 | - | 0.194 | 0.443 | 0.500 |
| BOLU (NS)-12/11/99 | 7.2, 10.3, D | 56 | 8.5 | 19 | 41 | - | - | 38 | 38 | - | - | 0.018 | 0.023 |
| BOLU (EW)-12/11/99 | 7.2, 10.3, D | 56 | 8.5 | 19 | 40 | 22 | - | 21 | 21 | - | - | 0.002 | 0.002 |
| BINGOL (NS)-01/05/03 | 6.5, 5.7, C | 65 | 20 | 28 | 46 | 27 | 27 | 27 | 27 | - | 0.000 | 0.006 | 0.008 |
| BINGOL (EW)-01/05/03 | 6.5, 5.7, C | 65 | 20 | 28 | 45 | 10.4 | - | 9.3 | 9.4 | - | - | 0.023 | 0.026 |
| TCU052 (NS)-20/09/99 | 7.6, 0.0, C | 90 | 28 | 52 | 70 | 720 | 718 | 721 | 713 | - | 0.003 | 0.006 | 0.022 |
| TCU052 (EW)-20/09/99 | 7.6, 0.0, C | 90 | 30 | 40 | 70 | 497 | 495 | 498 | 491 | - | 0.002 | 0.008 | 0.024 |
| TCU068 (NS)-20/09/99 | 7.6, 0.0, C | 90 | 29 | 43 | 68 | 854 | 854 | 866 | 865 | - | 0.000 | 0.022 | 0.040 |
| TCU068 (EW)-20/09/99 | 7.6, 0.0, C | 90 | 31 | 43 | 63 | 710 | 711 | 705 | 713 | - | 0.002 | 0.014 | 0.024 |
| TCU076 (NS)-20/09/99 | 7.6, 2.8, C | 90 | 24 | 46 | 63 | 72.6 | 72.6 | 72.5 | 75.9 | - | 0.000 | 0.019 | 0.142 |
| TCU076 (EW)-20/09/99 | 7.6, 2.8, C | 90 | 21 | 50 | 66 | 154 | 148 | 159 | 141 | - | 0.034 | 0.090 | 0.190 |
| TCU102 (NS)-20/09/99 | 7.6, 1.5, C | 90 | 24 | 57 | 70 | 115 | 115 | 117 | 115 | - | 0.000 | 0.034 | 0.034 |
| TCU102 (EW)-20/09/99 | 7.6, 1.5, C | 90 | 24 | 53 | 71 | 159 | 159 | 158 | 160 | - | 0.002 | 0.005 | 0.017 |
| TCU129 (NS)-20/09/99 | 7.6, 1.8, C | 90 | 24 | 48 | 66 | 74.3 | 67 | 79.1 | 71.7 | - | 0.100 | 0.131 | 0.297 |
| TCU129 (EW)-20/09/99 | 7.6, 1.8, C | 90 | 24 | 52 | 65 | 127 | 127 | 126 | 151 | - | 0.004 | 0.040 | 0.297 |

Table 2.

Arithmetic mean and coefficient of variation (COV) for the residual displacements from the suite of 100 baseline-corrected accelerograms, for the three baseline-variation noise models M2 through M4. Only one displacement time series is associated with the deterministic noise model M1. The mean residual displacements of Wu and Wu (2007), co-seismic deformations from GPS measurements (Yu et al., 2001), and distance between the GPS and the accelerograph station are given in the last three columns for comparison.

| Record | Arithmetic Mean of Residual Displacement (cm) | | | | Abs(COV) of residual displacement | | | Mean Residual Displacement (cm) | GPS Displacement (cm) | GPS-Accelerograph Station Separation (km) |
|---|---|---|---|---|---|---|---|---|---|---|
| | M1 | M2 | M3 | M4 | M2 | M3 | M4 | (Wu and Wu, 2007) | | |
| LDEO0375 (NS)-12/11/99 | 28 | 15 | 52 | 29 | 0.931 | 0.870 | 4.160 | | | |
| LDEO0375 (EW)-12/11/99 | 26 | 24 | 35 | 16 | 0.210 | 0.500 | 2.320 | | | |
| BOLU (NS)-12/11/99 | - | - | 8.2 | 8 | - | 0.170 | 0.210 | | | |
| BOLU (EW)-12/11/99 | 6.6 | - | 5.6 | 5.7 | - | 0.040 | 0.050 | | | |
| BINGOL (NS)-01/05/03 | 7.9 | 7.9 | 8.3 | 8 | 0.000 | 0.050 | 0.070 | | | |
| BINGOL (EW)-01/05/03 | 8.5 | - | 3.3 | 3.4 | - | 0.070 | 0.080 | | | |
| TCU052 (NS)-20/09/99 | 650 | 646 | 652 | 635 | 0.003 | 0.013 | 0.060 | 688 | 845 | 2.7 |
| TCU052 (EW)-20/09/99 | 375 | 384 | 386 | 379 | 0.003 | 0.010 | 0.031 | 358 | 342 | 2.7 |
| TCU068 (NS)-20/09/99 | 540 | 576 | 589 | 587 | 0.000 | 0.035 | 0.069 | | | |
| TCU068 (EW)-20/09/99 | 593 | 588 | 582 | 590 | 0.003 | 0.018 | 0.031 | | | |
| TCU076 (NS)-20/09/99 | 10 | 11 | 23 | 5.7 | 0.445 | 0.633 | 6.010 | 28 | 32 | 1.3 |
| TCU076 (EW)-20/09/99 | 132 | 134 | 146 | 124 | 0.037 | 0.096 | 0.304 | 87 | 88 | 1.3 |
| TCU102 (NS)-20/09/99 | 100 | 101 | 105 | 102 | 0.000 | 0.045 | 0.047 | 68 | 66 | 1.8 |
| TCU102 (EW)-20/09/99 | 66 | 64 | 63 | 65 | 0.006 | 0.025 | 0.093 | 87 | 59 | 1.8 |
| TCU129 (NS)-20/09/99 | 55 | 47 | 58 | 32 | 0.140 | 0.216 | 1.583 | | 32 | 2.1 |
| TCU129 (EW)-20/09/99 | 99 | 109 | 97 | 130 | 0.041 | 0.183 | 0.596 | | 88 | 2.1 |

Table 3.

Variability in the 1999 Chi-Chi mainshock co-seismic displacements from closely located GPS stations. The four stations are on the hanging wall of the fault and are all about the same distance from the surface rupture of the fault (GPS values from Yu et al., 2001)

| GPS Station | Distance from AF27 (km) | N Displacement (cm) | E Displacement (cm) |
|---|---|---|---|
| AF27 | 0.0 | 411 | -428 |
| M314 | 2.1 | 504 | -513 |
| AF25 | 4.3 | 535 | -401 |
| M345 | 6.1 | 649 | -606 |

# List of Figures

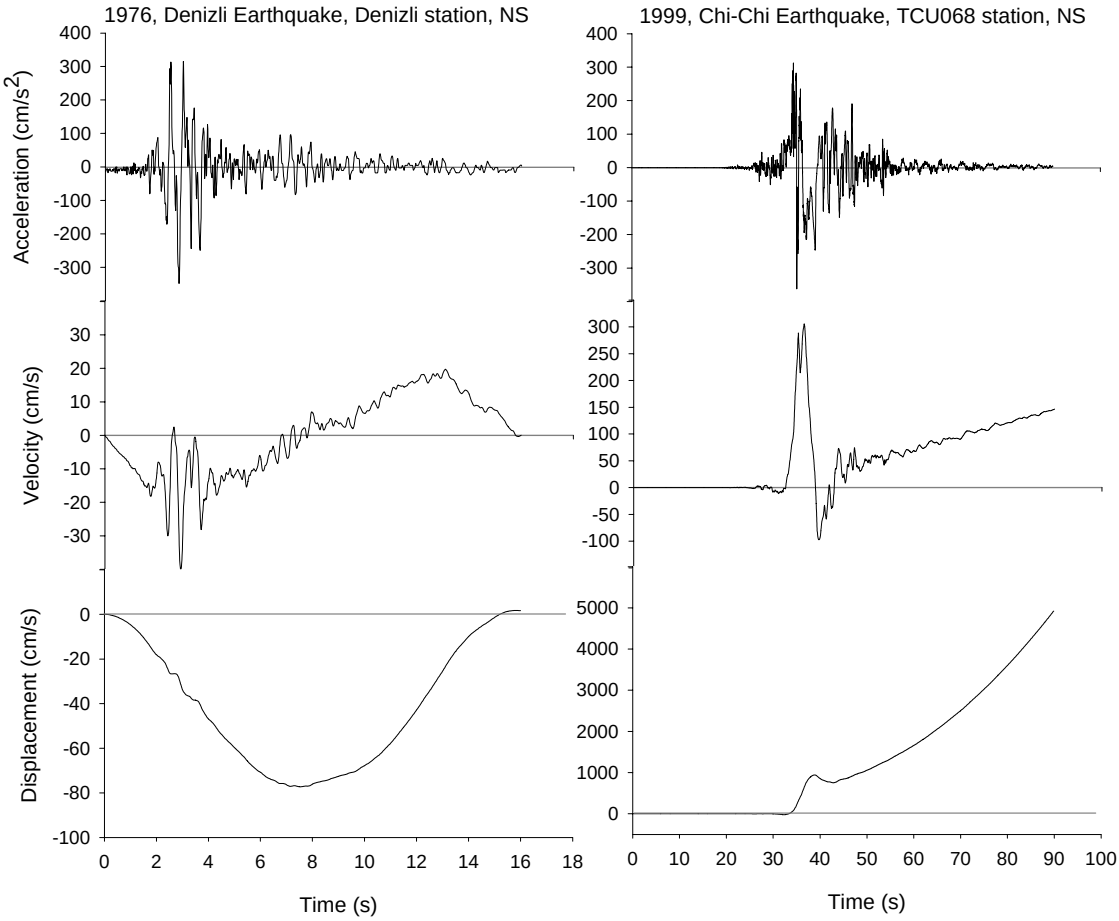


**Figure 1**. Different characteristics of long-period noise in the analog (left panel) and digital (right panel) accelerograms. Both accelerograms are zeroth-order-corrected: the mean of the entire record is removed from the analog accelerogram, whereas the mean of the first 15 seconds is subtracted from the whole accelerogram in the digital recording.

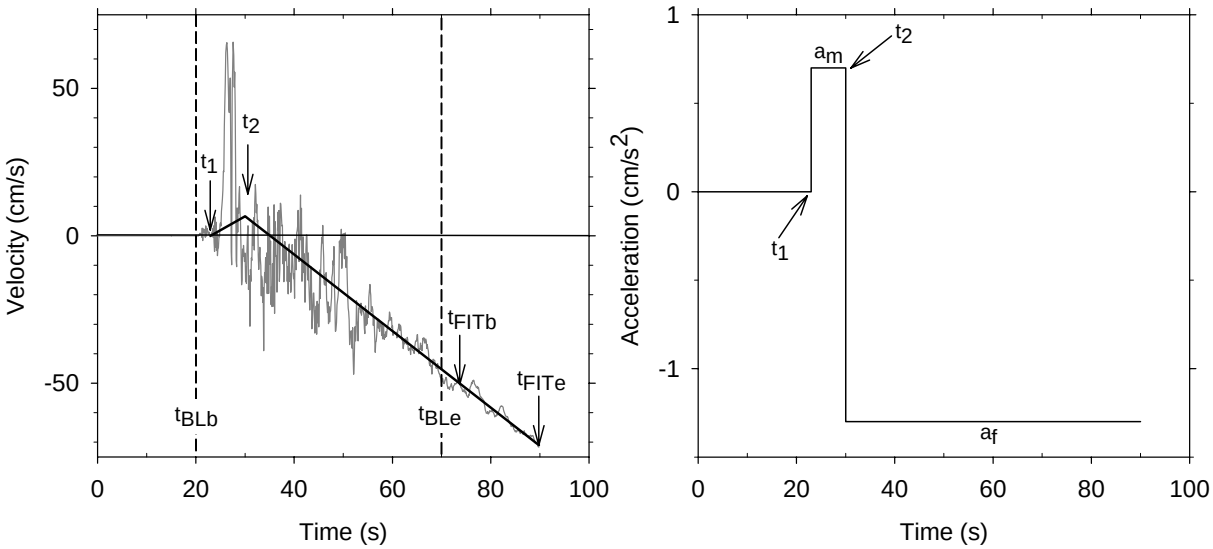


**Figure 2**. Description of important parameters in the modified Iwan method. The linear trend in the final segment of the velocity derived from the zeroth-order-corrected acceleration is the common feature of long-period noise observed in many digital accelerograms. The complex baseline variations are assumed to take place between times $t_1$ and $t_2$ and their cumulative effect is represented by a single acceleration shift $a_m$. The acceleration shift between times $t_1$ and $t_2$ is followed by another constant offset, $a_f$, that is determined by a linear line fitted to the zoc velocity. The linear fit is done between the time interval [$t_{FITb}$, $t_{FITe}$] where, in general, $t_{FITe}$ is taken as the end of the record ($t_{END}$). In the modified Iwan method, $t_1$ and $t_2$ can take values between the interval [$t_{BLb}$, $t_{BLe}$] provided that $t_2 > t_1$. A proposed methodology for the determination of the times $t_{FITb}$, $t_{BLb}$ and $t_{BLe}$ is presented in the text.

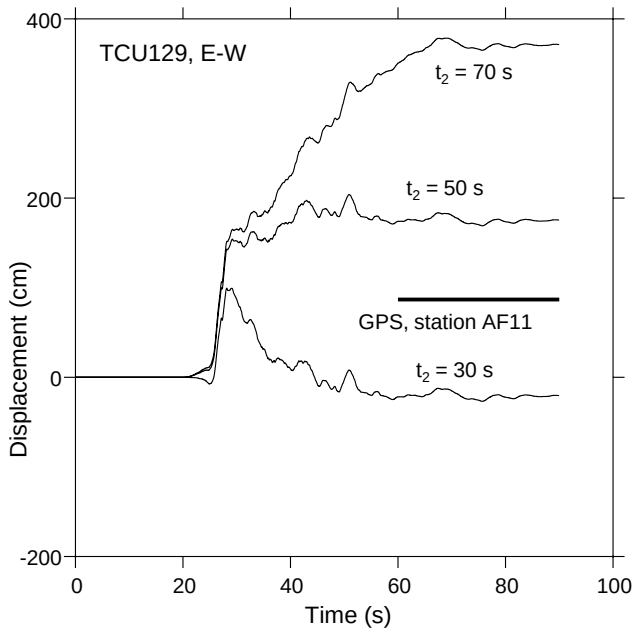


**Figure 3**. Displacements obtained from double integration of acceleration after baseline correction using the modified Iwan method, for three values of the parameter $t_2$. The GPS station providing the estimate of co-seismic residual displacement was 2.1 km from the recording station TCU129. (We made no attempt to choose $t_2$ so that the residual displacement matched the GPS value, although it is obvious that such a value could have been found, probably near 40 s.)

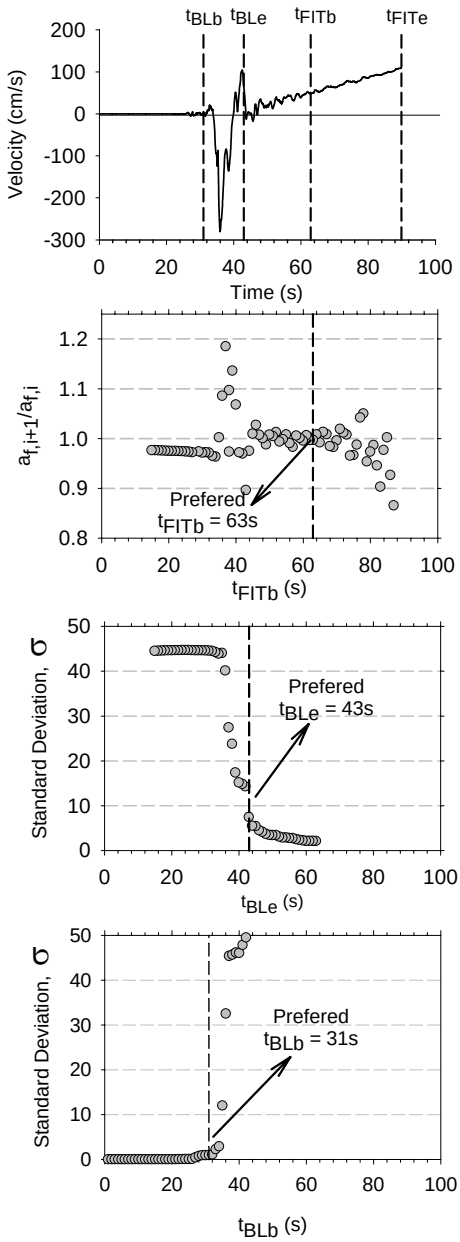


**Figure 4**. Illustration of the iterative procedure for choosing times needed in our simulation-based baseline-correction procedure, using the TCU068-EW record. The upper graph shows the velocity derived from the zeroth-order-corrected acceleration ("zoc velocity") and the time values to be used in our baseline-offset simulations, as computed from the iterative method. The second graph displays slope ratios of straight lines fitted iteratively to the zoc velocity time series between the times $t_{FITb}$ and $t_{END}$ (see text). Each point corresponds to the slope ratio between the consecutive iterations. The iterations used a series of $t_{FITb}$ decreasing in value (i.e., working toward the beginning of the record from the end). The time at which these ratios attain a relatively constant level of unity suggests the preferred location of $t_{FITb}$. The third and fourth graphs show the basis for choosing $t_{BLe}$ and $t_{BLb}$: the variation of standard deviations of the difference between the zoc velocity and the linear trend determined earlier (extending the trend toward decreasing time, starting from $t_{END}$) and between the zoc velocity and the zero line (extending toward increasing time, starting from the beginning of the record) for $t_{BLe}$ and $t_{BLb}$, respectively. The rapid change in the standard deviation values suggests the location of $t_{BLe}$ and $t_{BLb}$. The time, $t_{FITe}$ is taken as the end of the record ($t_{END}$).

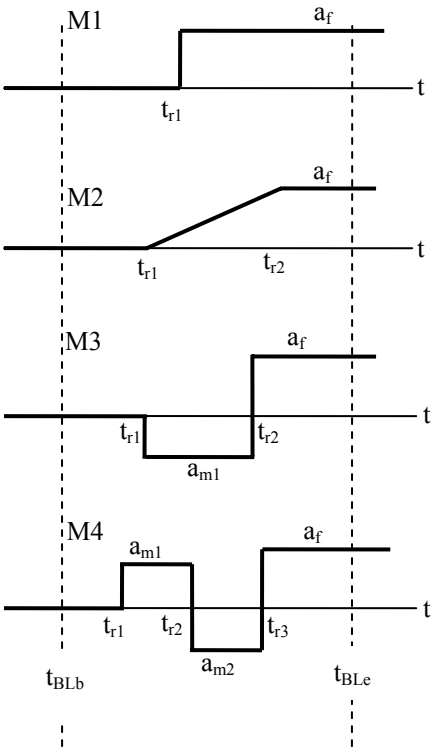


**Model 1 (M1):**

- $t_{r1} = -v_0/a_f$
- Constraints: $t_{r1} > t_{BLb}$
- $t_{r1} < t_{BLe}$

**Model 2 (M2):**

- $t_{r1}$ is randomly generated between $t_{BLb}$ and $t_{BLe}$.
- $t_{r2} = -2\times v(t_{BLe})/a_f + (2\ t_{BLe} - t_{r1})$
- Constraints: $t_{r2} > t_{r1}$ and $t_{r2} < t_{BLe}$

**Model 3 (M3):**

- $t_{r1}$ is randomly generated between $t_{BLb}$ and $t_{BLe}$.
- $a_{m1}$ is randomly determined ($|a_{m1}| \leq 2a_f$)
- $t_{r2} = 1/(a_{m1} - a_f) \times (v(t_{BLe}) + a_{m1}\times t_{r1} - a_f\times t_{BLe})$;
- Constraints: $t_{r2} > t_{r1}$ and $t_{r2} < t_2$

**Model 4 (M4):**

- $t_{r1}$ and $t_{r2}$ are randomly generated between $t_{BLb}$ and $t_{BLe}$.
- $a_{m1}$ and $a_{m2}$ are randomly determined ($|a_{m1}| \leq 2a_f$, $|a_{m2}| \leq 2a_f$)
- $t_{r3} = 1/(a_{m2} - a_f) \times (v(t_{BLe}) - a_{m1}\times t_{r2} + a_{m1}\times t_{r1} + a_{m2}\times t_{r2} - a_f\times t_{BLe})$;
- Constraints: $t_{r2} > t_{r1}$ and $t_{r2} < t_{BLe}$

**Figure 5**. Representative sketches of acceleration baseline-offset noise models. The models are abbreviated as M1 (Model 1), M2 (Model 2), M3 (Model 3) and M4 (Model4). In this study M1 is the simplest noise model whereas M4 represents the most complex noise model. The parameter $a_f$ is the slope of the straight line determined from the final portion of the zoc velocity time series (common in all noise models). Other constraints for establishing the key parameters of each noise model are presented on the right hand side of the plots.

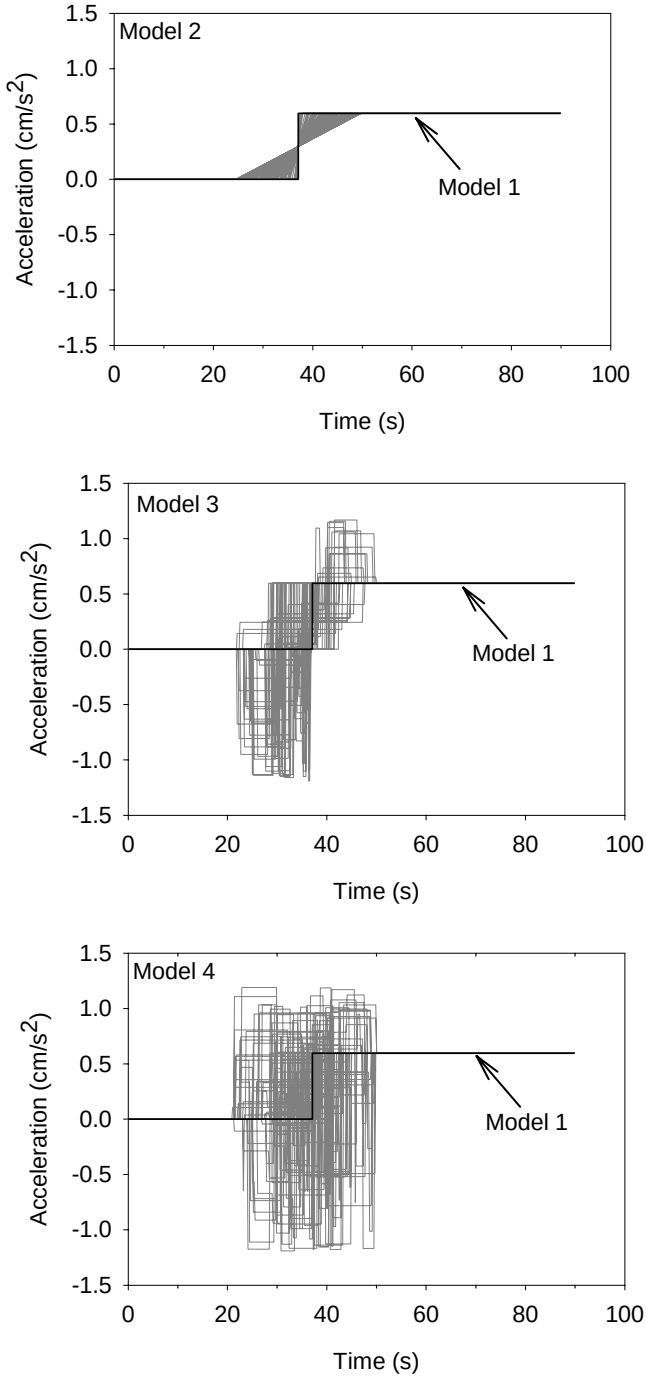


**Figure 6**. An illustrative case of the Monte Carlo simulations for the acceleration baseline-offset noise models considered in this study. 100 simulations are shown. The offset for the deterministic noise model M1 (for which there is no random variability) is superimposed in all plots for comparative purposes.

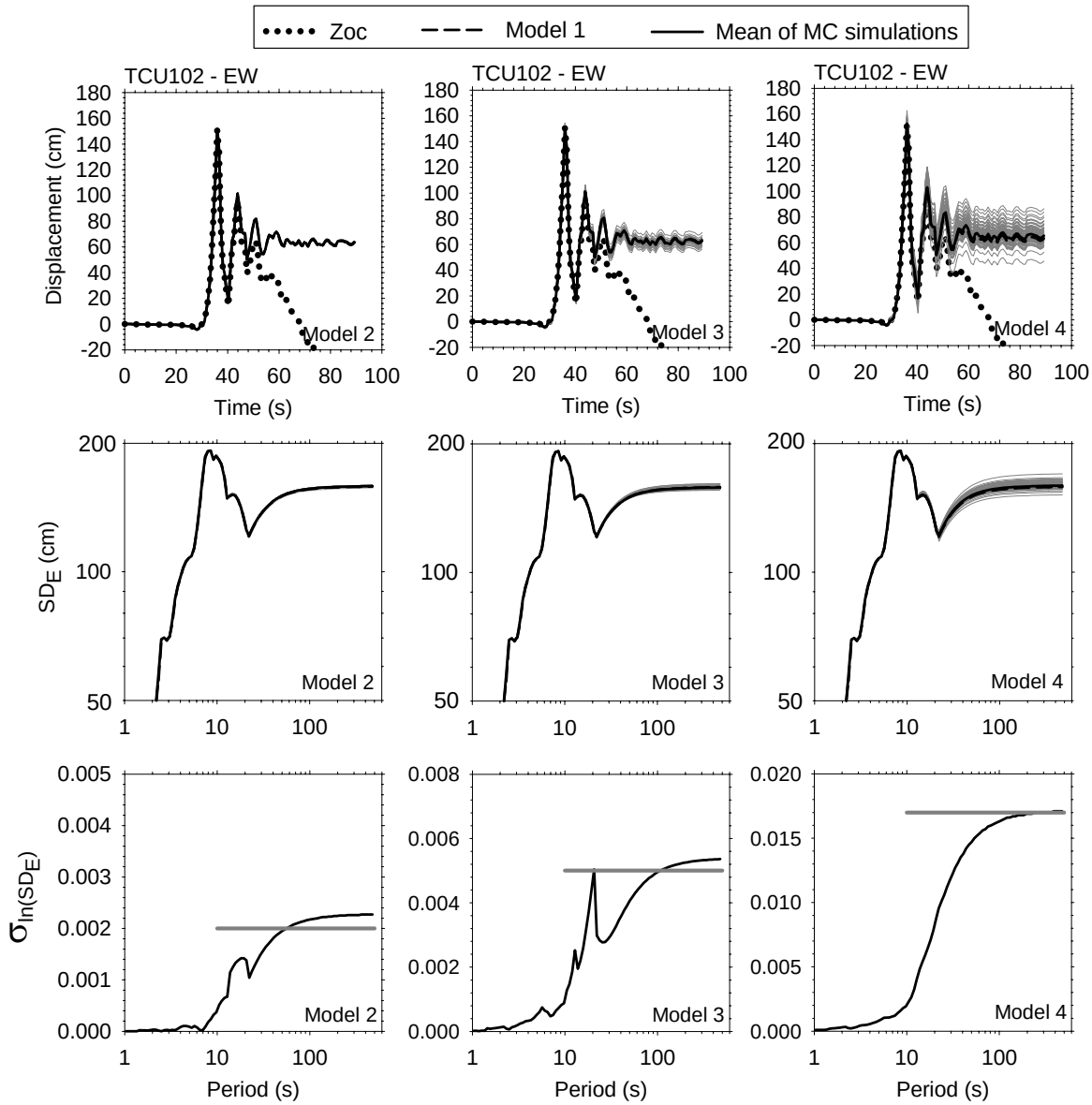


**Figure 7**. Estimated ground displacements (upper row) and elastic displacement spectra ($SD_E$) (middle row) corresponding to baseline corrections computed using the Monte Carlo (MC) simulations of acceleration baseline variations, for the EW component of TCU102. The graphs in the last row show the period-dependent standard deviations of the logarithm of $SD_E$. Columns from left to right show the simulation results of noise models 2, 3 and 4. The simulations are in dark grey. The ground displacement and spectrum plots also display the results for the zoc acceleration (dotted) (for which $SD_E$ is almost the same as for the M1 model), the mean of the Monte Carlo simulations (black solid line), and the results from the simplest noise model M1 (dashed black lines, invisible in this case as they are covered by the black solid lines). The horizontal gray line in the bottom row of graphs is $\sigma_{\ln(PGD)}$. The record used in this example does not possess a significant dependence of $SD_E$ on the noise mode.

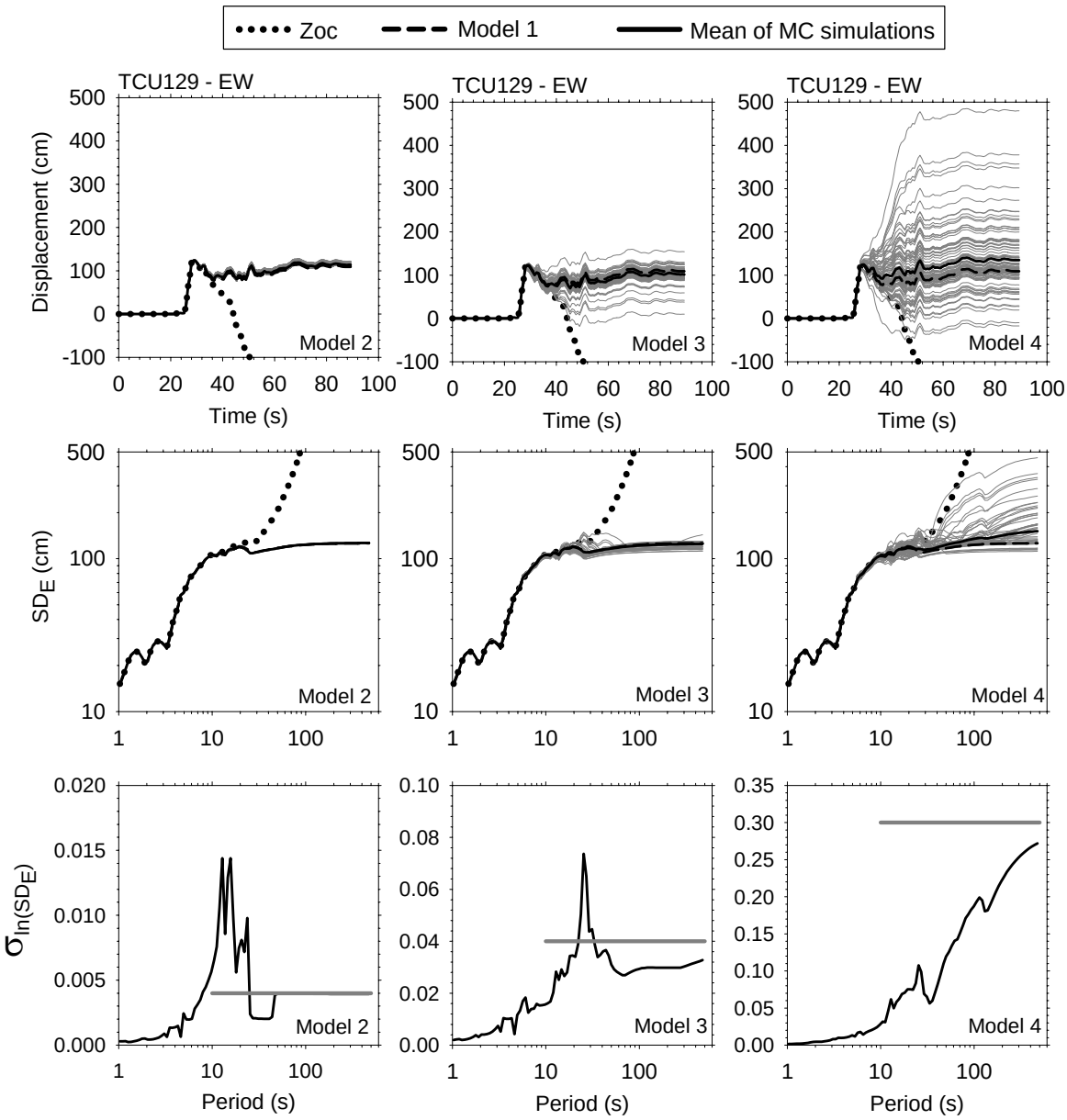


**Figure 8**. Similar to Figure 7, but using the EW component of TCU129. The record used in this example has a moderate dependence of the long-period $SD_E$ on the noise model. (Note that the curves pertaining to Model 1 are not visible in many panels as they are covered by black solid lines).

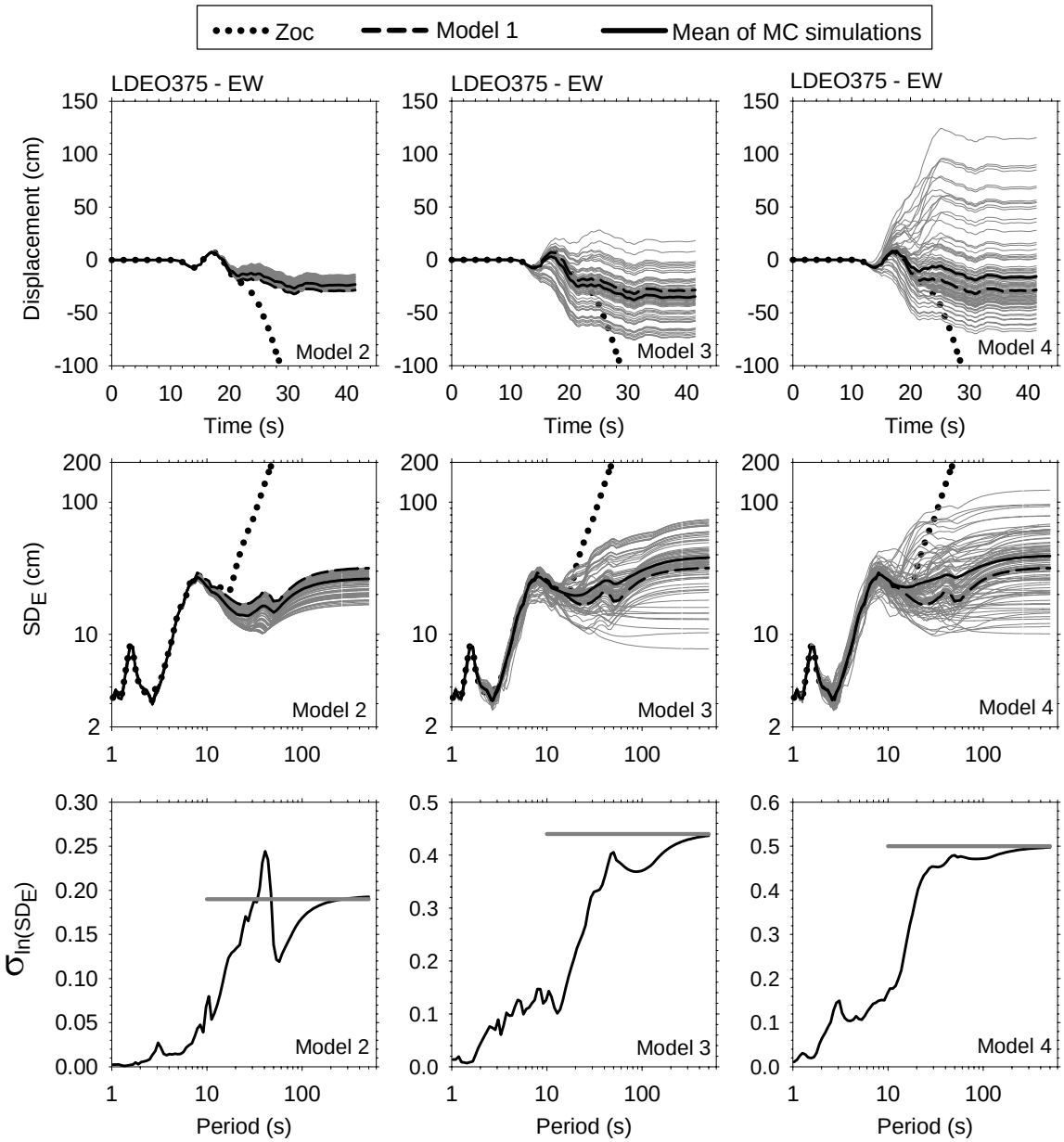


**Figure 9**. Similar to Figure 7, but using the EW component of LDEO375. The record used in this example has a significant dependence of the variability of long-period $SD_E$ on the noise model.

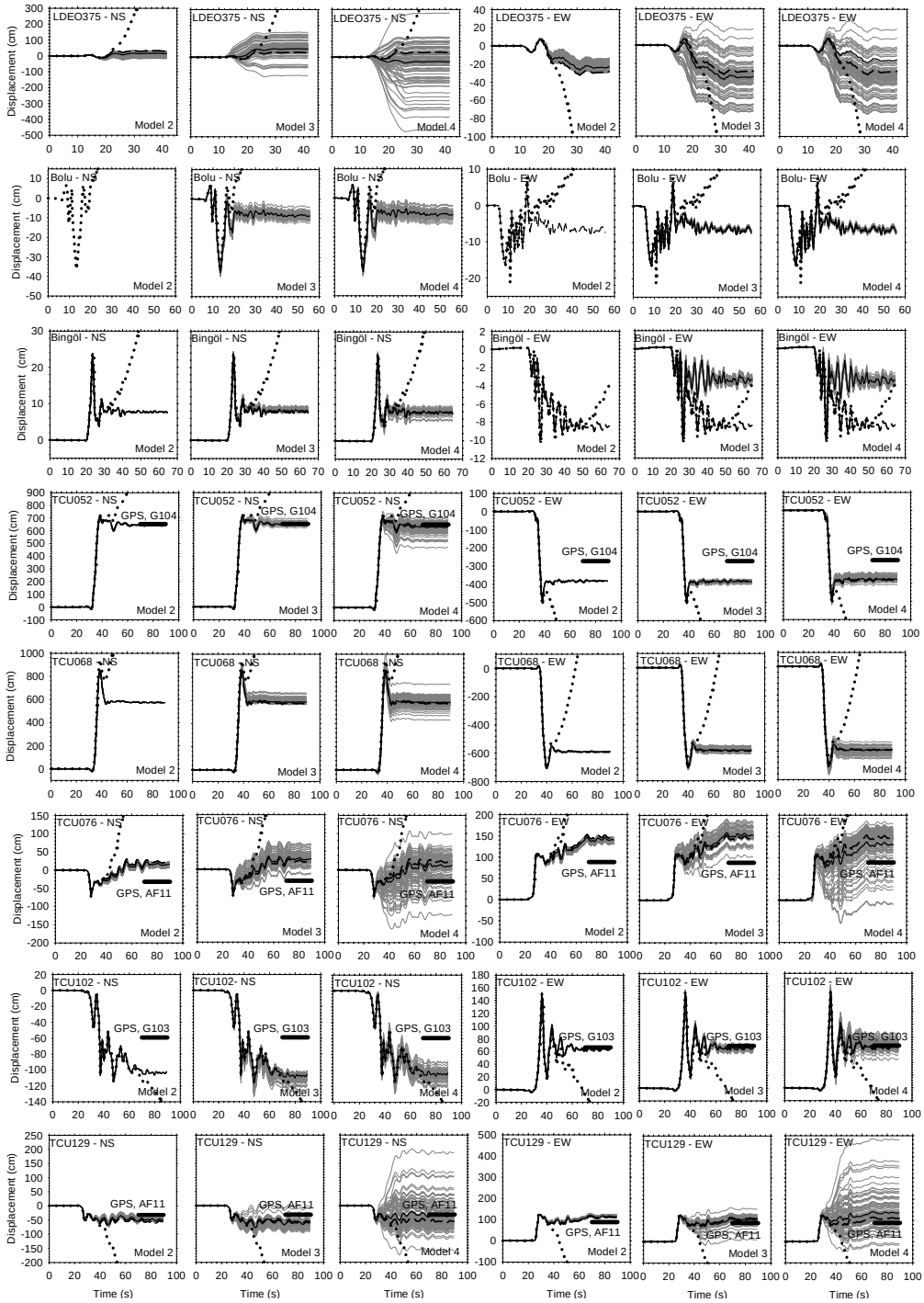


**Figure 10**. The displacement time series from the baseline-corrected accelerations for the entire dataset. Gray lines show the result from the baseline corrections obtained using the Monte Carlo simulations, black solid lines define the mean variation of the gray lines, and black dashed lines display the ground displacements for noise mode M1. The zoc displacements are given by the dotted lines. Some available GPS co-seismic deformation measurements are shown by heavy black horizontal line segments (although as discussed in the text, the GPS stations are not collocated with the accelerograph stations, and significant spatial variation in the residual displacements can exist).

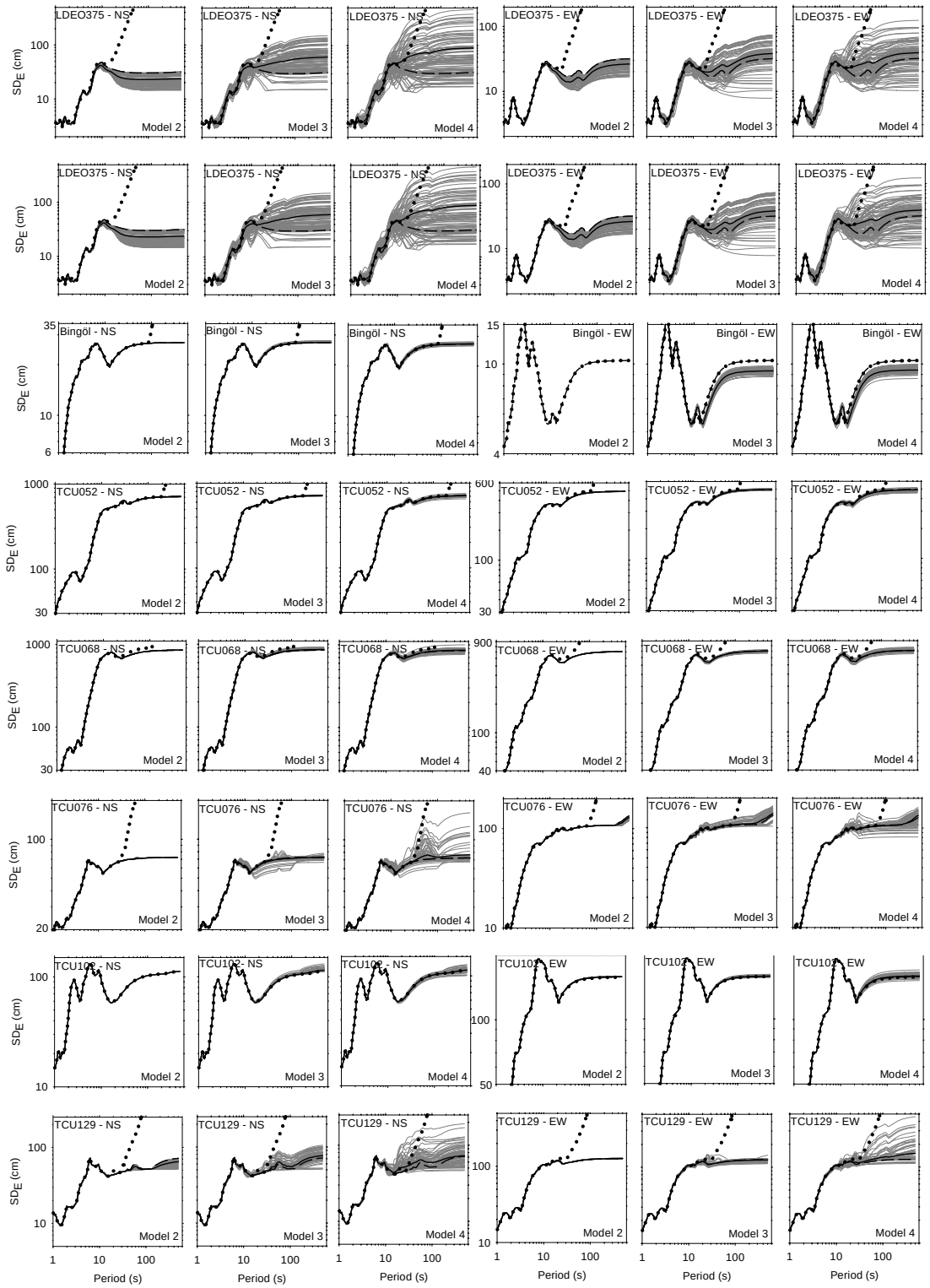


**Figure 11**. Variations in the elastic spectral displacements ($SD_E$) from the baseline-corrected accelerations due to different noise models, for the entire data set. Dark gray lines show the result from the baseline corrections obtained using the Monte Carlo simulations, black solid lines are the means of the $SD_E$ from the baseline-corrected accelerations, and black dashed lines display $SD_E$ for noise model M1. The plots also display the zoc $SD_E$ as dotted lines.

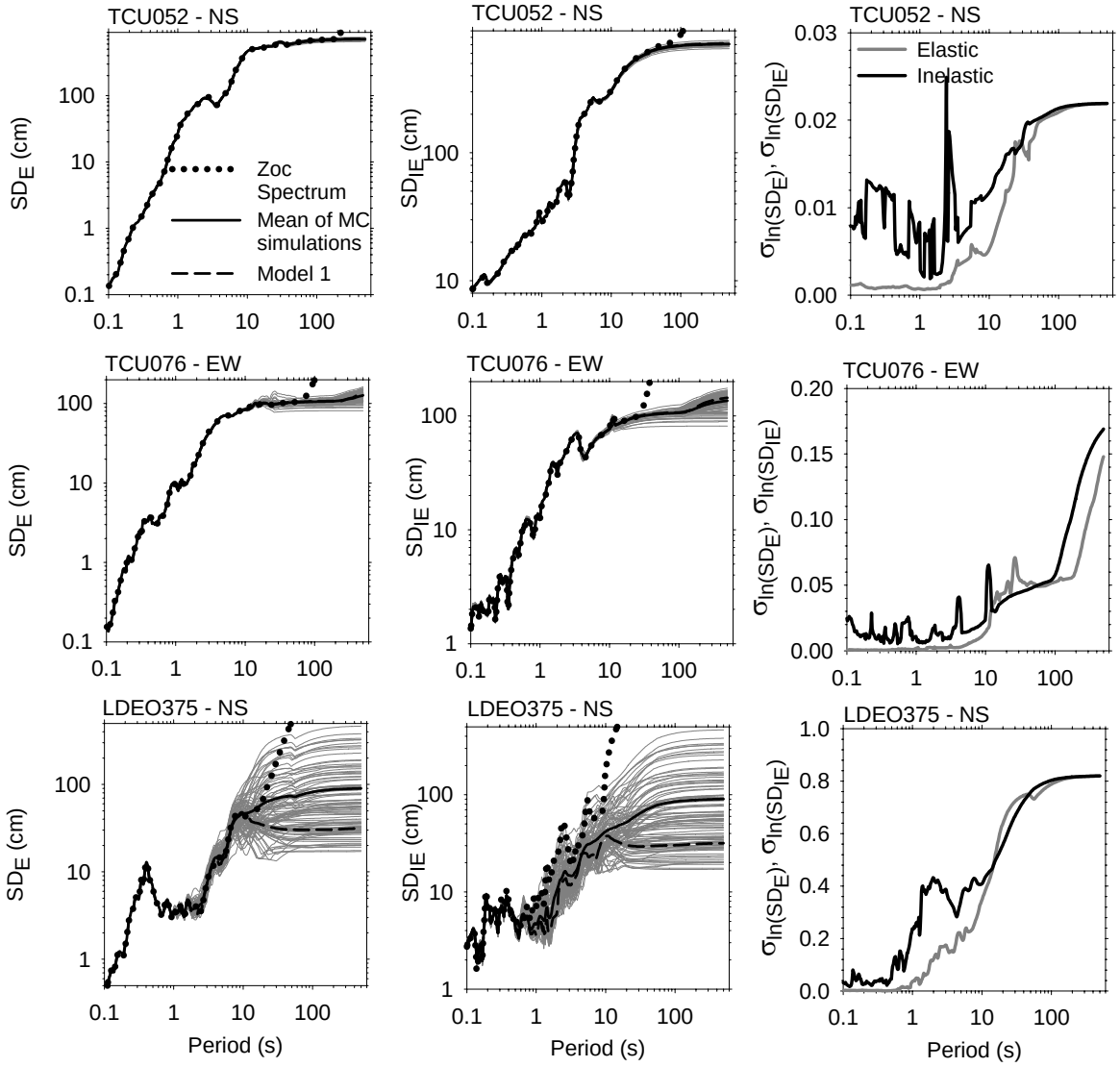


**Figure 12**. Comparisons of elastic (left panel) and inelastic (middle panel) spectral displacements from the baseline-corrected accelerations using the M4 noise model. Each row displays the results from a particular record with different levels of sensitivity to the noise model. The results using the M4 baseline corrections are shown in dark gray (results are shown for 100 simulations). The solid black lines in the spectral plots represent the mean of the M4 results whereas the dashed black lines and dotted curves show the results of the spectral displacements using the M1 and zoc baseline corrections, respectively. The rightmost panel gives the period-dependent elastic (gray) and inelastic (black) dispersions (standard deviations of the natural logarithm of simulated spectral displacements) for each record.

# Appendix

## The Relation of Variations in Displacements to Those in Long-Period Displacement Response Spectra

The residual displacement of an accelerogram can be sensitive to the correction used to remove the noise due to baseline changes in the acceleration time series. Large variations in residual displacements for a given acceleration time series, however, do not necessarily appear as corresponding variations in long-period elastic displacement response spectra ( *SD* ) of the baseline-corrected (blc) accelerograms. At first thought this might seem paradoxical, but it must be recalled that the long-period displacement response spectral ordinates are equal to the peak ground displacement ( *PGD* ) corresponding to the acceleration time series used to compute the response spectrum. Thus the *SD* s for a suite of corrections for a given accelerogram would have little or no variation at long periods if the peak displacement had little dependence on the correction procedure, even if the residual displacements showed considerable variation. Some examples will make this clear. Figure A1 shows zeroth-order-correction (zoc) and blc displacements and the corresponding *SD* . The zoc displacement diverges from the later part of the blc displacement, but because it trends upward, the peak displacement is the same for both time series. As a result, the *SD* for both time series is the same. If the zoc displacement had turned down, rather than up, the *PGD* would be different and this would show up as a difference in *SD* . This is what happened for the example shown in Figure A2. The zoc displacement trends downward, the peak displacement is for the two time series are different, and there are differences in the long-period *SD* . A final example is given in Figure A3, in which the zoc displacement again trends downward, but because the peak displacement on the blc record is positive, the negative displacement of the zoc displacement at the end of the record is still less in absolute value (100 cm) than the peak positive displacement (150 cm), and thus the *SD* shows no difference for the two time series.

The realization that it is the *PGD* that controls the long-period *SD* makes it easy to look at the displacement plots for a series of baseline corrections applied to a given record and predict whether there will be much effect on *SD* . For example, Figure A4 shows the blc displacements and the *SD* for our noise model 4, for TCU052 NS: the range of residual displacements is about a factor of 1.5, but the range of long period *SD* is about a factor of

1.15 because the *PGD* is little affected by the various baseline corrections. This can be contrasted with this case shown in Figure A5, but even here the variation of *SD* is much smaller than the variation of residual displacements. The comparisons in Figure A5 also explain why the distribution of long-period *SD* can be so nonsymmetrical about the mean value: only those displacement time series for which the residual displacements are equal or greater to the earlier *PGD* will show up as increases in the long-period part of the *SD*. Many of the residual displacements in Figure A5 reduce *PGD* slightly, if at all, and thus there is a mass of *SD* values near or slightly below the mean SD at long periods. The outliers, with either large positive or negative residual displacements, all contribute to long-period *SD* above the mean value.

An additional topic is what to expect for motions with significant near- and intermediate-field terms? If the complete waveform is thought of as the sum of a portion without a near-field ramp-like step (the "far-field" displacement) and a portion with a ramp-like step (the "near- and intermediate-field" displacements), and if the step starts near the beginning of the motion and has a rise time comparable to the strong motion duration, as seems reasonable from physical grounds, then the time of the peak far-field displacement will correspond to a portion of the step rise function that is well below its maximum offset. Thus the range of the peak displacement for a series of residual offsets will be less than the variation in the residual displacements, and for this reason the *SD* will show less variation than for the residual displacements.

In conclusion: if the *PGD* varies little for different baseline corrections applied to a given accelerogram, there will be little variation in *SD*, even if the residual displacements are very different for the suite of corrections.

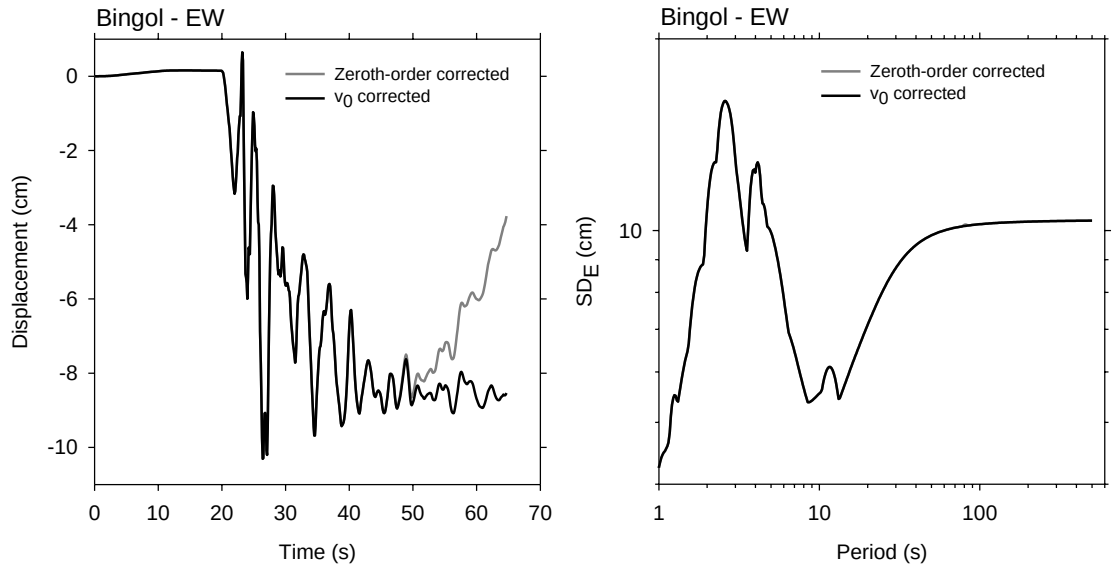


**Figure A1**. Zoc and v0-corrected displacements and the corresponding 5%-damped elastic displacement response spectra for a record for which there is no discernable variation in the long-period spectral response.

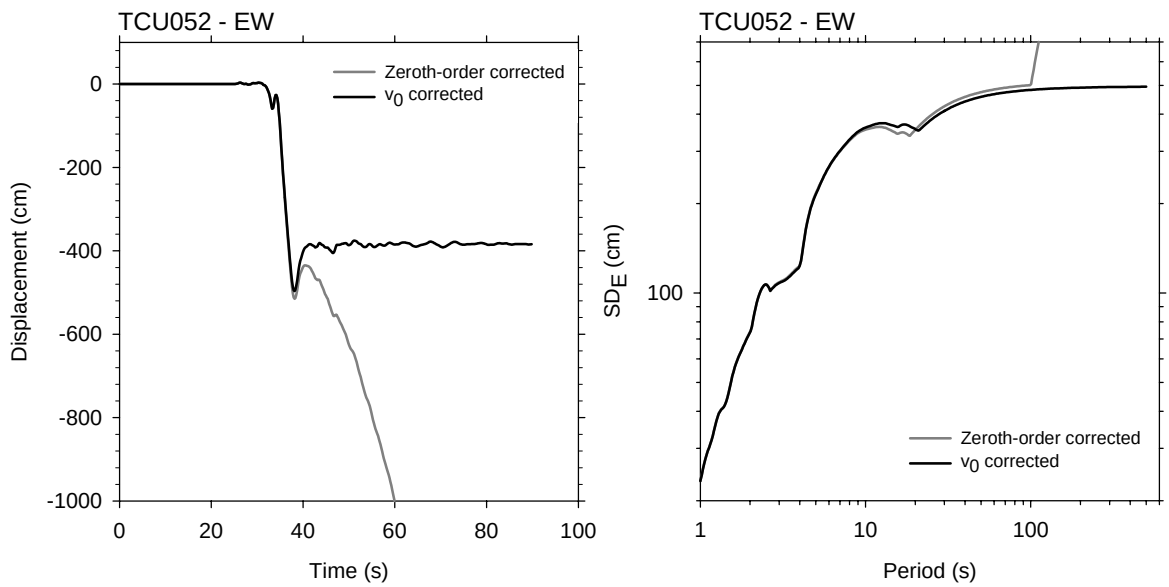


**Figure A2**. Zoc and v0-corrected displacements and the corresponding 5%-damped elastic displacement response spectra for a record for which there is a small variation in the very long-period spectral response.

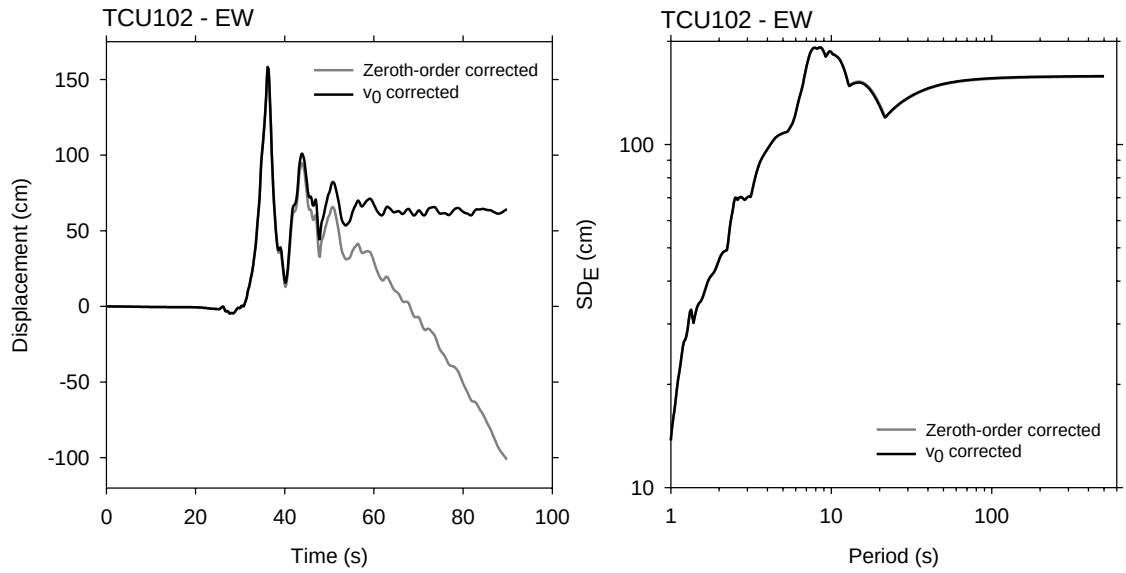


**Figure A3**. Zoc and v0-corrected displacements and the corresponding 5%-damped elastic displacement response spectra for a record for which there is no discernable variation in the very long-period spectral response, although the displacement wave forms differ significantly.

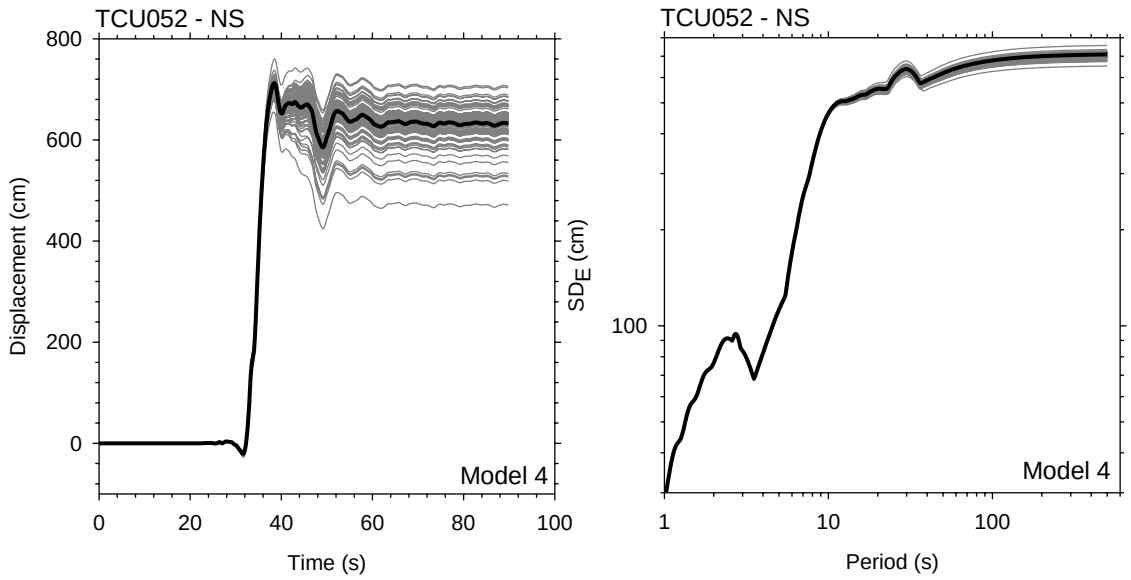


**Figure A4**. (gray) A series of baseline-corrected displacements and the corresponding response spectra; (black) the mean of gray curves. The small amount of variation in peak ground displacement leads to a correspondingly small amount of variation in the long-period response spectra, although there is a large variation in residual displacements.

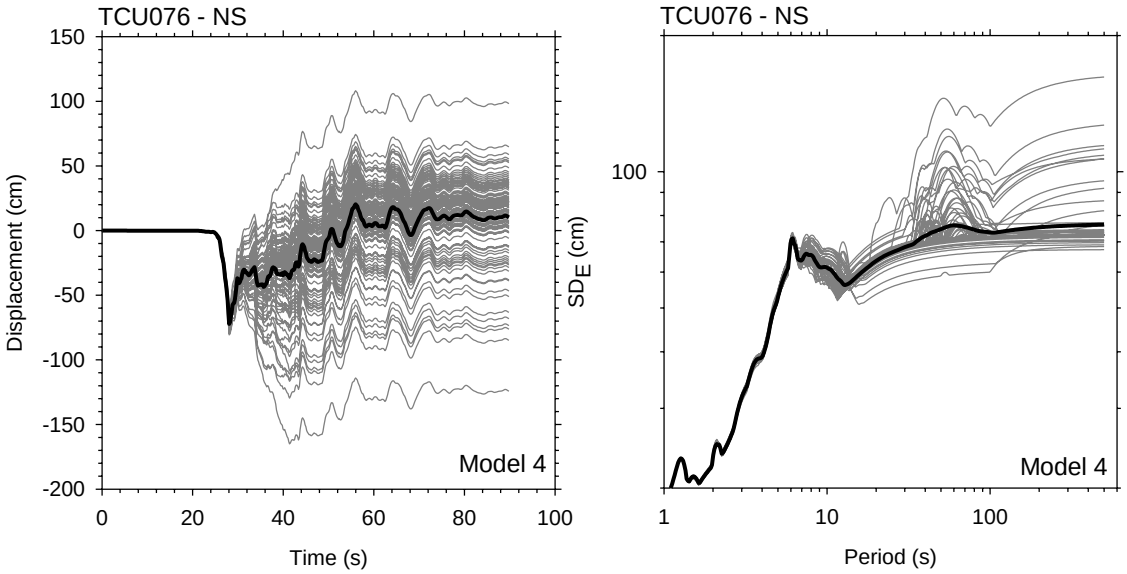


**Figure A5**. (gray) A series of baseline-corrected displacements and the corresponding response spectra; (black) the mean of gray curves. The large variation in peak ground displacement leads to a correspondingly large (and asymmetrical) variation in the long-period response spectra.